



CHALMERS
UNIVERSITY OF TECHNOLOGY

Boosting all-optical wavelength conversion efficiency using an AlGaAs-on-insulator Fabry-Perot microresonator without data rate limits

Downloaded from: <https://research.chalmers.se>, 2025-05-11 10:56 UTC

Citation for the original published paper (version of record):

Ye, C., Zhao, P., Liu, Y. et al (2025). Boosting all-optical wavelength conversion efficiency using an AlGaAs-on-insulator Fabry-Perot microresonator without data rate limits. *APL Photonics*, 10(4). <http://dx.doi.org/10.1063/5.0239950>

N.B. When citing this work, cite the original published paper.

RESEARCH ARTICLE | APRIL 21 2025

Boosting all-optical wavelength conversion efficiency using an AlGaAs-on-insulator Fabry–Perot microresonator without data rate limits ^{EP}

Chaochao Ye ^{ID} ; Ping Zhao ^{ID} ; Yang Liu ^{ID} ; Xinda Lu ^{ID} ; Chanju Kim ^{ID} ; Kresten Yvind ^{ID} ; Peter A. Andrekson ^{ID} ; Minhao Pu [✉] ^{ID}

 Check for updates

APL Photonics 10, 046115 (2025)
<https://doi.org/10.1063/5.0239950>



Articles You May Be Interested In

Expanding the quantum photonic toolbox in AlGaAsOI

APL Photonics (September 2022)

Hybrid InGaP nanobeam on silicon photonics for efficient four wave mixing

APL Photonics (December 2019)

The *infinity-loop microresonator*: A new integrated photonic structure working on an exceptional surface

APL Photonics (May 2023)

09 May 2025 14:25:39



Your One-Stop Shop for the Best Brands in Optics

- Extensive inventory with over 34,000 products available & 2,900 new products
- Fast shipping from our 9 distribution centres around the globe
- Bringing 80+ years of optical expertise to customers worldwide

Edmund optics | worldwide Shop Now

Boosting all-optical wavelength conversion efficiency using an AlGaAs-on-insulator Fabry–Perot microresonator without data rate limits

Cite as: APL Photon. 10, 046115 (2025); doi: 10.1063/5.0239950

Submitted: 23 September 2024 • Accepted: 4 April 2025 •

Published Online: 21 April 2025



View Online



Export Citation



CrossMark

Chaochao Ye,¹  Ping Zhao,^{2,3}  Yang Liu,¹  Xinda Lu,¹  Chanju Kim,¹  Kresten Yvind,¹ 
Peter A. Andrekson,²  and Minhao Pu^{1,a)} 

AFFILIATIONS

¹ DTU Electro, Department of Electrical and Photonics Engineering, Technical University of Denmark, Building 343, DK-2800 Kgs. Lyngby, Denmark

² Photonics Laboratory, Department of Microtechnology and Nanoscience, Chalmers University of Technology, 41296 Gothenburg, Sweden

³ College of Electronics and Information Engineering, Sichuan University, 610065 Chengdu, China

^{a)} Author to whom correspondence should be addressed: mipu@dtu.dk

ABSTRACT

Four-wave-mixing (FWM) based wavelength conversion offers a versatile solution for flexible optical networks. Significant research has focused on developing new materials and structures to enhance FWM performance. However, high-efficiency waveguide-based wavelength converters typically require either long interaction lengths or high pump power, which in turn limits their phase-matching bandwidth and complicates integration with on-chip lasers. Although microring resonator-based wavelength converters can substantially improve conversion efficiency (CE), they suffer from reduced signal bandwidth due to the resonance filtering effect. In this work, we propose a Fabry–Perot Bragg grating cavity-based singly resonant FWM scheme to enhance CE without compromising the signal bandwidth. In this configuration, only the pump light is resonantly enhanced within the cavity, while the signal and idler light undergo a single pass. We achieve CE enhancements of 16.7 dB in such a cavity compared to a waveguide with the same length on the AlGaAs-on-insulator platform with a phase-matching bandwidth exceeding 200 nm. We also demonstrate a continuously tunable wavelength conversion system, showcasing its potential to support high signal data rates. Our approach provides a promising pathway for on-chip laser-driven nonlinear signal processing, enabling efficient high-speed wavelength conversion and applications where both high CE and data rate are crucial.

© 2025 Author(s). All article content, except where otherwise noted, is licensed under a Creative Commons Attribution-NonCommercial-NoDerivs 4.0 International (CC BY-NC-ND) license (<https://creativecommons.org/licenses/by-nc-nd/4.0/>). <https://doi.org/10.1063/5.0239950>

I. INTRODUCTION

The invention of optical fiber connected people from all over the world, turning the globe into a small village. As the demand for the internet and mobile phones increases, the need for high-speed and energy-efficient signal processing becomes more pressing in the optical communication system. Traditionally, the optical signal is processed in the electrical domain by optical-to-electrical conversion, significantly limiting the data bandwidth and generating

excessive energy consumption. Consequently, all-optical signal processing (OSP) attracts intense attention as it addresses the power efficiency and speed constraints inherent in its electrical counterpart.¹ A pivotal function within the OSP is wavelength conversion, which enables all-optical reconfigurability of wavelength-division-multiplexing networks.² In addition, wavelength conversion can compensate for the optical fiber nonlinearities³ and open up new communication wavelength bands.⁴ A commonly employed scheme to achieve wavelength conversion is based on the four-wave-mixing

(FWM) effect. It provides the advantage of transparency to modulation formats with a nearly instantaneous response on the femtosecond scale.⁵

High-performance FWM was previously achieved in highly nonlinear fibers. However, hundreds of meters of fiber were required due to low material nonlinearity.⁶ Over the past decade, integrated nonlinear photonic waveguides have exhibited significantly higher effective nonlinearity than that of silica fibers and allow lithographically tailored dispersion, making it promising to achieve highly efficient and broadband chip-based FWM.⁷ The heterogeneous integration technology⁸ further enables the combination of lasers and nonlinear materials on a single chip, facilitating the realization of a fully integrated wavelength converter and unlocking practical applications. Various integrated nonlinear photonic platforms have been explored to achieve highly effective nonlinear processes.⁹ In low-index material platforms with large bandgaps, such as Si₃N₄, the weak light confinement leads to a relatively low effective nonlinearity.^{10–12} Although 100 Gbps wavelength conversion with a conversion efficiency (CE) of up to -0.6 dB has been demonstrated on the Si₃N₄ platform, it requires a waveguide length of more than 1 m and an operating power exceeding 1 W.¹⁰ In the case of high-index material platforms, such as silicon-on-insulator (SOI), CE is limited due to the two-photon absorption (TPA) in the telecommunication band.¹³ Therefore, finding a material platform with highly effective nonlinearity and low nonlinear loss is challenging. A recently developed AlGaAs-on-insulator (AlGaAsOI) platform stands out as a good candidate, offering large intrinsic nonlinearity, strong light confinement, and low linear and nonlinear material absorption.^{14,15} Based on a 3-mm-long AlGaAsOI waveguide, a CE of -4 dB was obtained at a pump power of 400 mW.¹⁶

However, waveguide-based wavelength converters still require high pump power operation, which is difficult to achieve with on-chip lasers. Novel device configurations need to be introduced to improve CE further, thereby reducing the pump power requirement. Microring resonators have been utilized to enhance CE by leveraging the large circulating power. For instance, a microring resonator demonstrated a remarkable 53-dB CE improvement compared to an equivalent-length waveguide (110 μ m) at the same pump power.¹⁷ However, the high-Q microresonators exhibit a narrow resonance linewidth, typically at the megahertz scale, which imposes significant limitations on handling broadband data signals, essential for high-speed optical signal processing. Coupled resonators have been proposed to break the signal bandwidth constraint of single resonators.^{18,19} However, the trade-off relationship between the enhancement factor and signal bandwidth persists, and improvement is achieved at the expense of increased structural complexity and footprint. The demonstrated microresonator-based wavelength converter still shows limited performance concerning the signal bandwidth, with the maximum data rate achieved being 40 Gbit/s.¹⁹ Therefore, achieving a high CE without signal bandwidth limitation remains a challenge.

Here, we propose using a Fabry–Perot Bragg grating (FPBG) cavity to achieve a singly resonant FWM process. Unlike microring resonators, which distribute resonant modes across the entire spectrum, the band-structured FPBG cavity confines resonant modes within a narrow photonic stopband.^{20–22} Consequently, the pump wavelength can be positioned to operate in a resonant mode within

the stopband, while the signal and idler waves can be situated outside the stopband. This approach enhances FWM efficiency compared to the waveguide-based device without sacrificing the operational signal bandwidth imposed by microring schemes. In this work, we achieved a CE enhancement of 16.7 and 10.2 dB in 1- and 3-mm-long FPBG cavities, respectively, compared to a bare waveguide counterpart. We also showed that the FPBG device can relax the length requirement, thereby increasing the phase-matching bandwidth. Using a 1-mm-long device, we achieved a conversion bandwidth of 214 nm, significantly larger than the 108 nm bandwidth of the 3-mm-long device, despite their similar CEs. Based on the FPBG-based wavelength converter, we also demonstrated continuous wavelength conversion with consistent performance, indicating potential for high-speed data rate operation.

II. STRUCTURE AND PRINCIPLE

Figure 1(a) presents the schematic of a singly resonant FWM-based all-optical wavelength conversion in an AlGaAsOI chip. The low-power continuous wave (CW) pumping light (green) and the data-encoded signals (blue) are simultaneously coupled into the FPBG cavity. Inside the cavity, the pump power accumulates to a high level while the signal pulse undergoes a single pass. The accumulated high pump power facilitates an efficient FWM process, replicating signal pulses to idler pulses at another frequency (red). The single-pass configuration for both the signal and idler ensures high-speed operation. Here, the FPBG cavity consists of two distributed Bragg reflectors (DBRs) positioned on both sides of a nonlinear waveguide. The DBR is implemented by introducing sinusoidal corrugations into a waveguide, as shown in Fig. 1(b). Each corrugation period corresponds to a unit cell in the DBR, characterized by its length (Λ), mean width (W), and corrugation depth (ΔW), as illustrated in Fig. 1(c). Figure 1(d) displays a scanning electron microscopy (SEM) image of one of our fabricated DBRs, where smooth boundaries are observed. The periodic corrugation of DBR induces a stopband where the pump light can be located. The length of the DBRs determines the reflectivity and coupling strength to the waveguide, influencing the intensity enhancement of the pump light. A critical coupling condition needs to be met to achieve maximum pump power enhancement. Thus, the output mirror reflectivity is designed to be close to 100%, and the input mirror reflectivity is adjusted by changing the number of periods to match the round trip loss of the cavity (see Fig. S1 of the [supplementary material](#)).

Next, we compared the CE of FWM under different resonant schemes. The frequency-domain nonlinear coupled-mode equations⁵ were used to calculate it numerically (see the [supplementary material](#)). In the undepleted pump regime, the CE is proportional to $(\gamma P_p L_{eff})^2$, where γ is the effective nonlinearity of the waveguide, P_p is the on-chip pump power, and L_{eff} is the waveguide's effective length.⁵ Figure 2(a) shows the calculated CE for a non-resonant waveguide device under different lengths (L) and loss (α), assuming the effective nonlinearity γ is $400 \text{ W}^{-1} \text{ m}^{-1}$ and the pump power P_p is 10 mW. The CE in the waveguide shows a strong dependence (quadratic scaling) on the waveguide's effective length. Achieving a higher CE necessitates a longer effective waveguide length. In contrast, a higher CE with a shorter length can be achieved in a microring resonator, where all three waves are on-resonant, as shown in

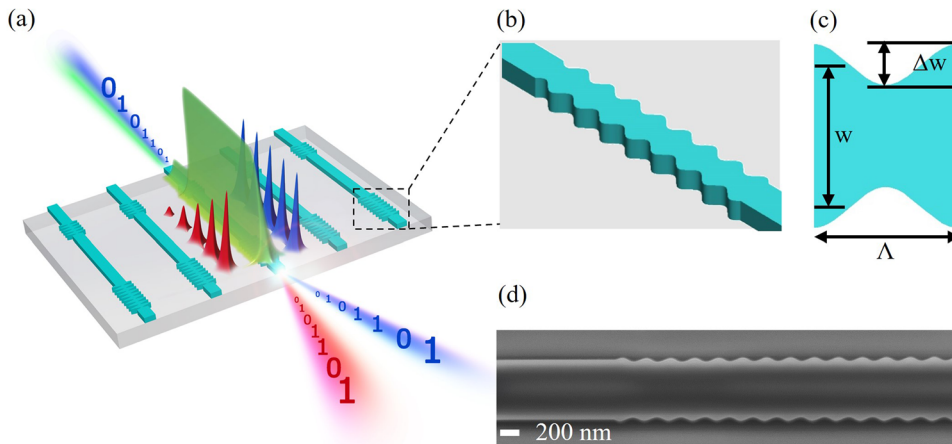


FIG. 1. (a) The schematic of FWM-based wavelength conversion in an AlGaAsOI FPBG cavity. (b) The schematic of the DBR structure. (c) The illustration of the unit cell of DBR. (d) The SEM picture of one of the fabricated DBRs.

Fig. 2(c). The CE is proportional to $(\gamma P_p L_{eff})^2 (IE_p)^2 (IE_s)(IE_i)$, where $IE_{p/s/i}$ represents the intensity enhancement in the cavity of the pump, signal, and idler light. However, the linewidth of the resonance will significantly limit the operated signal bandwidth. A critical coupling condition was assumed to achieve maximum pump power enhancement in the cavity. As shown in Fig. 2(c), the supported bandwidth is only 2.4 GHz for a 4 dB/cm waveguide loss. In contrast to the triply resonant FWM process, the FPBG cavity-enabled singly resonant scheme proposed in this work can break the CE-signal bandwidth constraints, as illustrated in Fig. 2(b). The

CE can be improved by a factor of $(IE_p)^2$ compared to the non-resonant scheme, while the signal bandwidth is no longer limited by the resonance linewidth compared to the triply resonant scheme. In the singly resonant scheme, half of the circulating pump power co-propagates and interacts with the single-pass signal during the FWM process. The pump light enhancement (IE_p) scales with both the device length and waveguide loss, following a trend similar to that observed in microresonators (as shown in Fig. S2). A shorter cavity length results in a larger IE_p , thereby alleviating the length requirement to achieve high CE for non-resonant waveguides [see Fig. 2(b)]

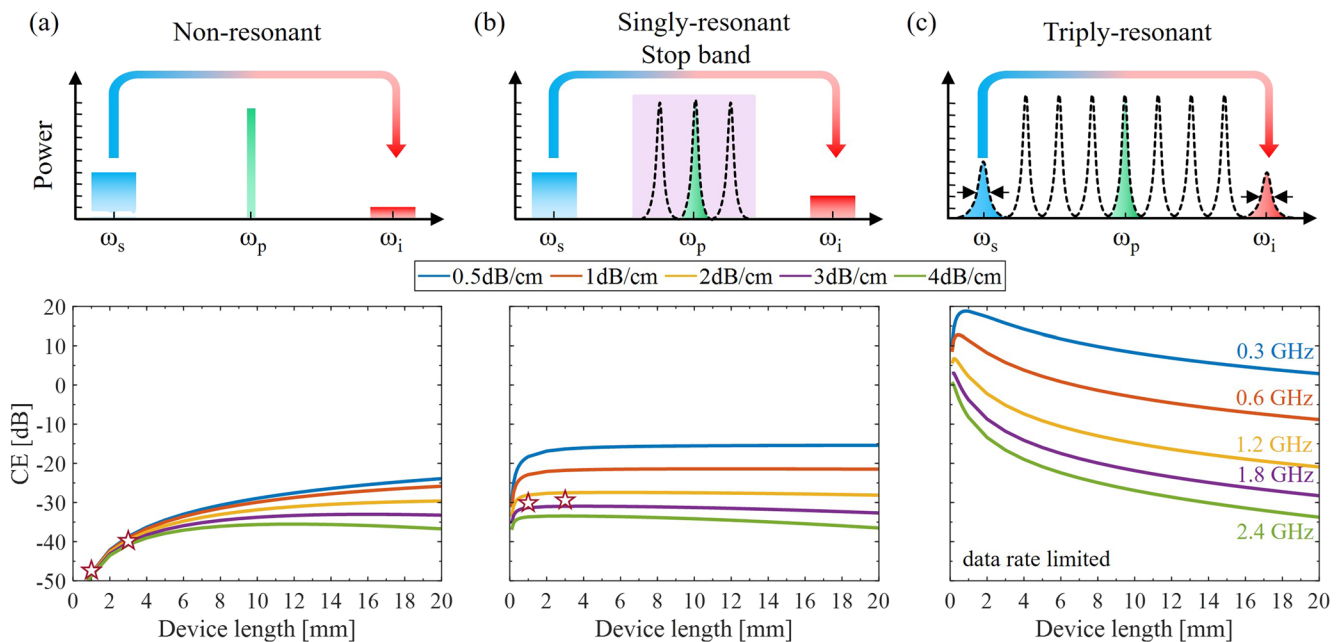


FIG. 2. Illustration of the FWM-based wavelength conversion (upper panel) and the corresponding calculated CE (lower panel) at a pump power of 10 mW with an effective nonlinearity of $400 \text{ W}^{-1} \text{ m}^{-1}$ under different resonant schemes: (a) non-resonant FWM based on a waveguide, (b) singly resonant FWM based on an FPBG cavity, and (c) triply resonant FWM based on a microring resonator. The star marks represent the corresponding experimental results.

and broadening the phase-matching bandwidth. Although the CE in this scheme is lower compared with the triply resonant scheme, the single-pass signal lifts the signal bandwidth limit imposed by the resonance linewidth. It should be noted that for ultra-broadband operation, radiation modes of the DBR with a much higher frequency than the stopband of the DBR may affect the phase-matching bandwidth (see Fig. S3). Nonetheless, the signal bandwidth (data rate) remains unaffected within the conversion bandwidth range.

III. RESULTS AND DISCUSSION

A. Device fabrication and linear characterizations

We experimentally demonstrated the FPBG cavity-based singly resonant FWM process in the AlGaAsOI platform. The 300 nm-thick AlGaAsOI wafer is prepared by wafer bonding and substrate removal processes.²³ The DBR mirrors and FPBG cavities are patterned using an optimized electron-beam lithography process and a boron trichloride (BCl₃)-based dry etching process. A 100-nm-thick Al₂O₃ and 3- μ m thick SiO₂ layers were deposited as the upper cladding using atomic layer deposition (ALD) and plasma-enhanced chemical vapor deposition (PECVD), respectively. The inverse tapered edge couplers have also been fabricated in the input and output waveguide ports to achieve efficient chip-to-fiber coupling. Manual cleaving was applied to the chip for edge coupling, and the average fiber-to-chip coupling loss was estimated to be around 2.5 dB/facet. To analyze the relationship between CE and the lengths of FPBG cavities, we fabricated two chips with waveguide lengths of 1 and 3 mm, respectively, on the same wafer sample.

A tunable external cavity laser and an optical power meter are synchronized with a 3 pm resolution to record the transmission and reflection spectrum of the devices simultaneously. A low-intensity TE-polarized light was launched into the devices to avoid thermal and nonlinear effects. The measured normalized transmission spectrum of DBRs with varied number of periods (N) is presented in Fig. 3(a), where the unit cell of the DBRs has dimensions of W = 800 nm, Λ = 290 nm, and ΔW = 50 nm. The central wavelength and bandwidth of the stopband are 1533 and 4 nm, respectively. We noted that the central wavelength deviates from the designed

1550 nm due to fabrication discrepancies. Figure 3(a) illustrates that the DBR mirror reflectivity can be adjusted by changing the number of periods. To achieve the critical coupling condition of the FPBG cavity, the period number of the output mirror was set to 800 to achieve a reflectivity of almost 100%, while the number of grating periods of the input mirror was varied to balance the round trip cavity loss. The measured reflection spectrum of a 1-mm long FPBG cavity is shown in Fig. 3(b), revealing an extinction ratio of up to 20 dB at the wavelength of 1533 nm, where the critical coupling condition is nearly satisfied. In this case, the input mirror was set to 500 periods. Figure 3(c) presents a typical resonance spectrum of fabricated FPBG cavities featuring a 1.06 GHz linewidth corresponding to a 2 dB/cm waveguide propagation loss.²⁴ The measured finesse for the 1- and 3-mm long FPBG devices are 36.7 and 12.2, respectively, corresponding to intracavity power enhancements of 10.7 and 5.9 dB at low pump power levels.

B. Nonlinear characterizations

We performed FWM experiments based on the 1- and 3-mm-long FPBG cavities and the waveguide counterparts fabricated on the chips. CW signals and pump waves were generated through tunable external-cavity lasers and combined using a WDM coupler. Both signal and pump waves were aligned with polarization controllers to the TE polarization of the AlGaAsOI waveguide. Lensed fibers were used to couple light into and out of the chip, and the output spectrum was recorded by an optical spectrum analyzer (OSA). Figures 4(a) and 4(b) show the measured FWM spectrum for these devices. The CE is -47 and -40.5 dB for 1- and 3-mm-long waveguides at a pump power of 9 mW, respectively. Here, the CE was obtained through the output spectrum, $CE_{\text{output}} = P_i(L)/P_s(L)$. As the maximum waveguide length is 3 mm, the propagation loss for the signal is negligible; therefore, we define the measured CE_{output} as the CE [$CE = P_i(L)/P_s(0)$] of the FPBG cavity. The measured CE for the straight waveguides is marked with a star symbol in Fig. 2(a), showing good agreement with the theoretical predictions. Due to the pump power enhancement in the FPBG cavities, the CEs are enhanced by 16.7 and 10.2 dB for the 1- and 3-mm devices, respectively. Here, it is worth mentioning that the resonances within the stopband have different extinction ratios, leading to varying IEs.

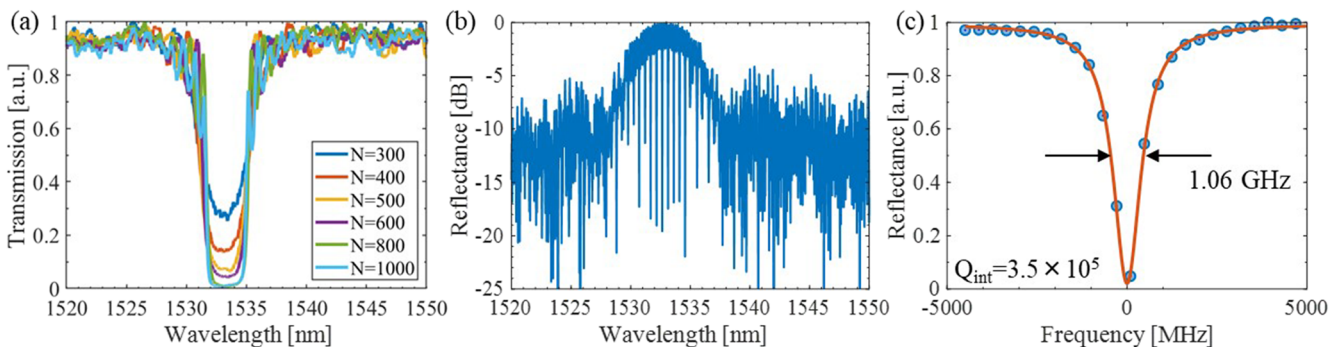


FIG. 3. (a) The measured transmission spectrum of the DBR ($W = 800$ nm, $\Lambda = 290$ nm, and $\Delta W = 50$ nm) with different number of periods (N). (b) The measured reflectance spectrum of the 1 mm-long FPBG cavity with 500 periods in the input mirror and 800 periods in the output mirror. (c) The typical resonance spectrum of the FPBG cavity.

09 May 2025 14:25:39

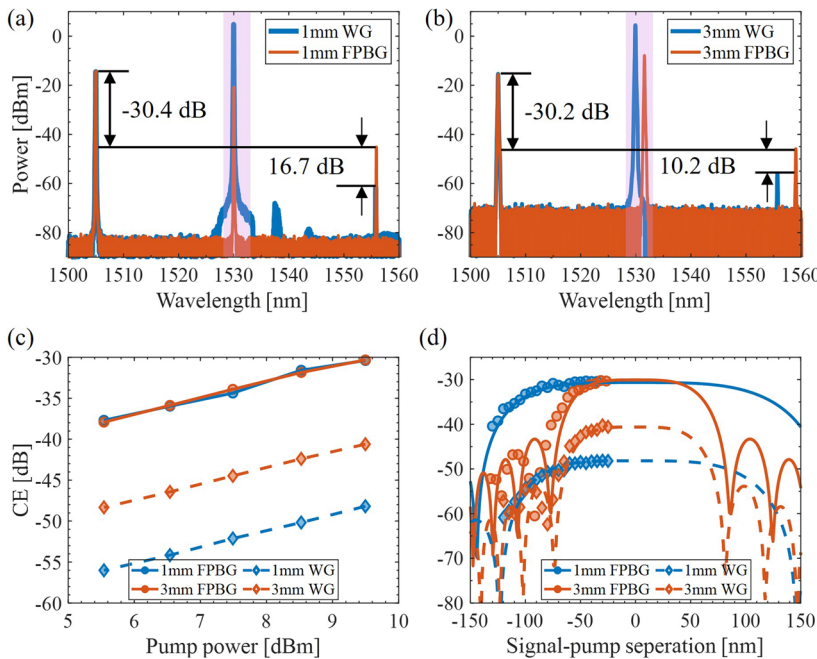


FIG. 4. (a) and (b) Measured FWM spectrum for the waveguide (blue) and FPBG cavity (orange) when the input on-chip power is 9 mW with the device length of (a) 1 mm and (b) 3 mm, respectively. The pink bar represents the stopband of the FPBG cavity. (c) Measured CE vs on-chip power without the use of EDFA. (d) Measured CE vs the signal-pump separation.

Therefore, the pump light was carefully tuned within the resonance supporting the largest IE by monitoring the generated idler power using the OSA to ensure maximum CE enhancement. To simplify the precise pump light tuning process, a broadband DBR with flat reflectivity is highly desirable in the future. The experimental results are labeled in Fig. 2(b). The CE of the FPBG-based devices becomes strongly dependent on the waveguide propagation loss while the length requirement is greatly relaxed. The minor discrepancy between the experimental result and theoretical prediction may be attributed to additional coupler losses from DBRs and variations in coupling conditions at high intracavity power levels.

The relationship of CE vs on-chip power was also investigated, as shown in Fig. 4(c). The CE follows a quadratic relation with the pump power, ranging from 5 to 10 dBm, without using an erbium-doped fiber amplifier (EDFA) to amplify the pump power. Based on the measurements of the 1- and 3-mm long waveguide devices, a linear function was used to fit the measured data. The dashed lines represent the fitting result from which an average effective nonlinearity of $400 \text{ W}^{-1} \text{ m}^{-1}$ is derived, which was utilized for the simulation in Sec. II. We noted that the device exhibits a lower effective nonlinearity compared to our previous work in Refs. 16 and 17 due to the differences in waveguide cross-sectional dimension. To assess the FWM enhancement provided by the FPBG, both straight waveguides and FPBG resonators with identical cross-sectional dimensions were fabricated on the same chip in this study. Figure 4(d) shows the CE of the FWM as a function of signal-pump wavelength separation (conversion bandwidth) for 1- and 3-mm waveguides and FPBG cavities. Due to limitations in laser availability, the smallest measurable signal-pump separation is ~ 25 nm. The injected on-chip pump power is kept at 9 mW. The measured CE bandwidth matches well with the simulated data for the 1- and

3-mm long waveguides at the pump power of 9 mW, showing a 3-dB bandwidth of about 179 and 103 nm. In contrast, the CE bandwidth for the 1- and 3-mm long FPBGs are 214 and 108 nm, respectively, corresponding to waveguide lengths of 0.7 and 2.7 mm. We note that the effective cavity length is less than the nominal device length since the DBR mirror has a reflection depth, which explains why the FPBG cavity CE bandwidth is slightly larger than the waveguide counterpart. Here, we emphasize that the cavity enhancement of the FPBG device enables a shorter nonlinear interaction length than the standard nonlinear waveguide when targeting the same CE. Consequently, the short length of the FPBG device will mitigate the impact of the phase mismatch, allowing for a wider conversion bandwidth.⁵

C. System demonstration of all-optical wavelength conversion for communications

We experimentally characterize wavelength conversion of broadband optical signals using a 3-mm-long FPBG AlGaAsOI chip to validate the device performance in nonlinear optical signal processing applications. The experimental setup is shown in Fig. 5(a). In the transmitter, the signal light emitted from an external-cavity laser is modulated by a Mach-Zehnder modulator to generate a 10 Gbit/s non-return-to-zero on-off-key (NRZ-OOK) data signal. The generated signal is coupled into the photonic chip-based wavelength converter, where a CW light at the resonance of around 1532 nm is used as the pump wave. An EDFA is used to adjust the pump power, and the amplified spontaneous emission (ASE) noise from the EDFA is filtered with a bandpass filter. The wavelength converter generates an idler light—a replica of the data-encoded signal light—through the degenerate FWM process. An OSA is used to monitor the generated idler light amplitude to ensure the pump

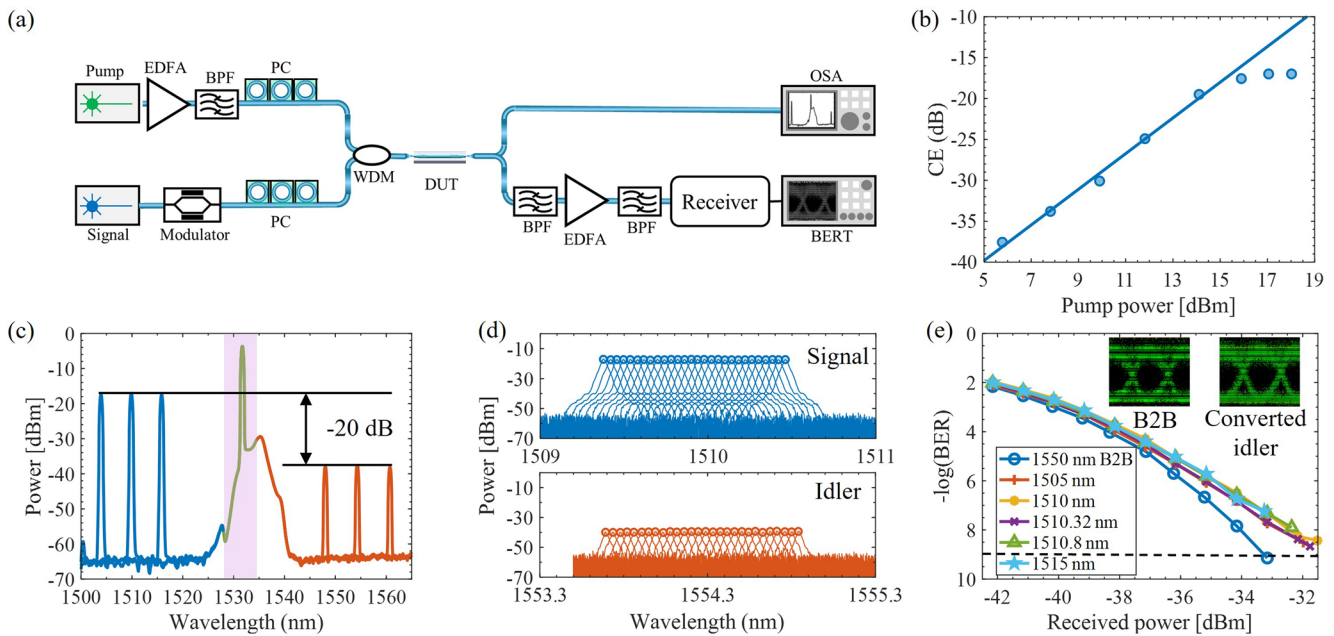


FIG. 5. (a) Experimental setup for all-optical wavelength conversion of a high-speed data signal using a nonlinear AlGaAsOI chip. (b) Measured CE vs pump power with the use of EDFA. (c) Measured FWM spectrum at different signal wavelengths of 1505, 1510, and 1515 nm when the pump wavelength is 1532 nm at the on-chip input power of 25 mW. The pink bar represents the stopband of the FPBG cavity. (d) Measured signal and idler spectrum by scanning the frequency of the signal light over 135 GHz. The consistent CE ensures wavelength conversion of data signals beyond 100 Gbaud. (e) Measured BER for the 10 Gbit/s back-to-back (B2B) and wavelength-converted data signal vs received optical power after bandpass filter (BPF). Inset: eye diagram of the back-to-back and the converted idler at BER of around 10^{-9} .

light is aligned with one of the cavity resonances. In the receiver, a bandpass filter rejects the pump and signal light and transmits the idler light. An EDFA was used to amplify the idler so that the optical power level is in the optimum detection range of the receiver. After that, a bandpass filter was used to filter out the ASE noise. The converted idler is finally sent to the bit-error-rate tester (BERT) for the BER evaluation.

Figure 5(b) shows the measured CE of the 3-mm-long FPBG device vs on-chip pump power, with an EDFA used to amplify the pump power. The CE begins to saturate when the pump power exceeds 16 dBm, despite the pump still operating in the undepleted regime. This saturation is accompanied by a reduction in the extinction ratio of the pump resonance, which may be attributed to increased nonlinear losses caused by surface states of the AlGaAs waveguides.^{25,26} The nonlinear loss depends not only on the input pump power but also on the intensity enhancement of the FPBG cavity. Due to the enhanced pump power within the cavity, saturation occurs at an intracavity pump power of 21 dBm for the FPBG device. In contrast, the waveguide device reported in Ref. 16 exhibits CE saturation at -4 dB when the on-chip power reaches 26 dBm. This discrepancy is likely due to increased nonlinear losses, which may arise from variations in wafer quality and fabrication processes. To reduce the nonlinear loss for a given input pump power in an FPBG device, one can increase the device length, thereby reducing the intracavity power. While lower intracavity power may initially decrease CE, the longer nonlinear interaction length for the single-pass signal wave compensates for this effect. Consequently, compared to shorter

devices with higher intracavity power and nonlinear loss, longer devices achieve improved CE. Moreover, implementing an effective surface passivation technique²⁷ could help mitigate surface state effects, thereby mitigating nonlinear losses. Further improvements in CE also require minimizing linear loss. One effective strategy is adopting deep ultraviolet (DUV) lithography with reflowed photoresist,²⁸ which can reduce scattering losses and enhance device performance. Here, we chose a pump power of 25 mW for the OSP experiment to avoid nonlinear absorption.

To show the signal wavelength tunability of the FPBG devices, we chose three signal wavelengths of 1505, 1510, and 1515 nm randomly to conduct the wavelength conversion experiment. Figure 5(c) shows the measured FWM optical spectrum at a pump power of 25 mW. We noted that the spectral shape of the pump light comes from the remaining ASE noise of the EDFA. A CE of -20 dB was obtained for these three signal wavelengths under such pump power. The nearly consistent CE indicates that this device is suitable for multi-wavelength conversion. The group velocity dispersion and the length of the cavity waveguide determine the wavelength conversion range. A shorter FPBG wavelength converter with an engineered higher-order dispersion can further improve the operation bandwidth.¹⁶ To further show the device's potential for high-speed operation, the signal carrier wavelength was scanned across a 135 GHz range with a dense frequency step, and the converted idler spectrum maintains a uniform amplitude in this range, as shown in Fig. 5(d), which is greatly larger than the reported engineered resonance linewidth of 40 GHz.¹⁹ In principle, the device

is suitable for high-speed operation. Here, we used a 10 Gbit/s data rate as an example. The measured BERs of the back-to-back signals at different wavelengths and the corresponding converted idlers are shown in Fig. 5(e), where the system power penalty of around 1 dB was achieved at the BER of 10^{-9} . The penalty may arise due to the unstable fiber-to-chip coupling. All the converted idlers have almost the same performance, further showing the high-speed operation potential of the FPBG-based wavelength converters.

D. FWM-based integrated wavelength converters discussion

We summarize the experimental results of the state-of-the-art FWM-based all-optical wavelength conversion achieved with different integrated photonic platforms and structures in Table I. In recent years, silicon photonics has attracted intense attention due to the compatibility of CMOS fabrication technology. Various passive and active components are investigated and demonstrated in the SOI platform to make the function of the photonic integrated circuits more powerful. The FWM-based wavelength converter was also successfully demonstrated in the SOI platform.^{13,29} However, the TPA-induced free carrier absorption (FCA) limits the ultimate CE. To mitigate the FCA effect, a p-i-n diode was utilized to remove the generated carriers, which helped to improve CE.³⁰ Nevertheless, it requires complex fabrication processes and limited freedom to change its waveguide layout, which increases the waveguide loss and fabrication cost and limits the dispersion engineering ability.

Therefore, other TPA-free integrated nonlinear material platforms have been developed, such as a-Si,³¹ As₂S₃,³² Hydrex,³³

Si₃N₄,¹⁰ and AlGaAs.¹⁶ Among them, AlGaAsOI exhibits the largest effective nonlinearity, making it a promising candidate for enabling a broadband and efficient FWM process. However, achieving a high CE still requires either a long waveguide length or high pump power. This makes it challenging to integrate the single-pass waveguide with the on-chip laser, preventing it from becoming a fully integrated wavelength converter. To further increase the effective nonlinearity, special waveguide structures such as slot waveguides³⁴ or plasmonic waveguides³⁵ have been employed to reduce the effective mode area. However, these waveguides exhibit high propagation loss, which limits their performance. Photonic crystal (PhC) waveguides utilizing the slow light effect have also been exploited, while the conversion bandwidth is smaller than 13 nm due to the narrow bandwidth of the PhC.³⁶ Microring resonators have also been used to enhance CE. However, the narrow resonance linewidth (on the order of megahertz) of high-Q microresonators limits the maximal data rate. Therefore, there are only a few demonstrations of the OSP in microresonators.^{17,37,39,40} Resonance linewidth engineering has been made recently, but the improvement is limited.^{18,19} So far, the highest data rate using a double-ring resonator is still only 40 Gbit/s.¹⁹ In this work, we proposed using an FPBG cavity to balance the trade-off between CE and the supported signal data rate.

Figure 6 shows the calculated CE vs data rate for different resonant structures—waveguide, microring resonator, and FPBG resonator in the AlGaAsOI platform. The lengths of the FPBGs and waveguides are set at 3 mm to ensure a conversion bandwidth of over 100 nm, as illustrated in Fig. 4(d), assuming waveguide losses

TABLE I. A summary of reported FWM-based wavelength conversion performance realized on integrated platforms. Note: γ : effective nonlinearity, α : waveguide loss, L : device length, P_p : on-chip pump power, CE: conversion efficiency, BW: conversion bandwidth, DDR: demonstrated data rate, and SDR: support data rate (which depends on RL: resonance linewidth, and the demonstrated maximum linewidth is 40 GHz).¹⁹

Device design	Material	γ ($W^{-1} m^{-1}$)	α (dB/cm)	L (mm)	P_p (mW)	CE (dB)	BW (nm)	DDR (Gbit/s)	SDR	Ref.
WG	Si	126 ^a	2.3	28	160	-10.6	19	10	BW	13
WG	Si	247 ^a	3-4	6	32	-28.49	60	10	BW	29
WG	p-i-n Si	30 ^a	0.3	30	457	-8.5	40	1024	BW	30
WG	a-Si	800 ± 50	3.7	1	70	-26	50	20	BW	31
WG	As ₂ S ₃	9.8	1	60	730	-27.5	40	40	BW	32
WG	Hydrex	0.22	0.07	500	158	-40	>10	32	BW	33
WG	Si ₃ N ₄	1	1.4	1420	1230	-0.6	27	128	BW	10
WG	AlGaAs	630	1.3	3	35.5	-23	750	1280	BW	16
Slot WG	Polymer	100	16	4	1340	-37	18	42.7	BW	34
Plasmonic WG	Polymer	7.7×10^4	NA	0.002	30 000	-13.3	60	NA	BW	35
PhC WG	Si	NA	NA	0.096	895	-33	<13	10	BW	36
MR	Si	NA	3	0.7	9	-30	NA	10	RL	37
MR	Si	NA	1.68	0.434	2.7	-15.57	400	NA	RL	38
CROW MR	Si	NA	2	0.63	16	-36	120	10	RL	18
MR	Si-graphene	NA	6	0.63	20	-38	20	10	RL	39
MR	Hydrex	NA	NA	0.302	165	-28.5	27	2.5	RL	40
MR	AlGaAs	720	2	0.110	32	-16	130	40	RL	17
Coupled MR	AlGaAs	720	4.5	0.453	1	-37.6	160	38	RL	19
FPBG	Si ₃ N ₄	0.99	0.36	0.39	5.3	-37.7	NA	NA	RL	21
FPBG	AlGaAs	400	2	1/3	25	-20	214/108	10	BW	This work

^aDerived value according to the available data provided in relevant references.

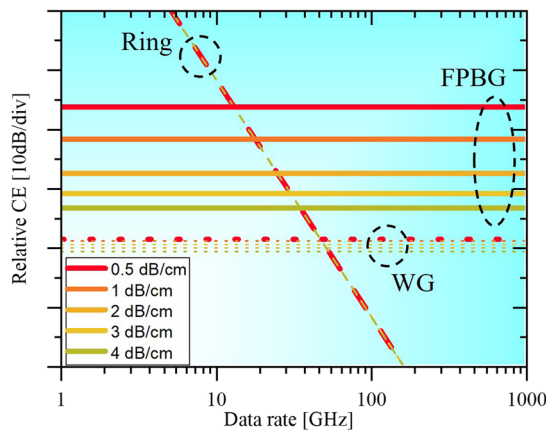


FIG. 6. Comparison of relative CE vs data rate for different resonant structures—waveguide (dotted line), FPBG resonator (solid line), and microring resonator (dashed lines) in the AlGaAsOI platform. The lengths of the FPBGs and WGs are set at 3 mm, while the length of the ring resonator is set at 110 μm to ensure they have a similar conversion bandwidth (~ 100 nm).¹⁷ Different waveguide losses of 0.5, 1, 2, 3, and 4 dB/cm (indicated by different line colors) are considered here.

of 0.5, 1, 2, 3, and 4 dB/cm. The length of the ring resonator is set at 110 μm to achieve a conversion bandwidth of ~ 100 nm.¹⁷ The power intensity enhancement depends on the resonance linewidth for the ring resonators, imposing a strict trade-off relationship between the CE and data rate. Although the single-pass waveguide-based devices support a large data rate, their CE is relatively low. The CE remains nearly consistent for different waveguide losses due to the short length of the waveguides. The triply resonant devices (ring resonators) exhibit higher conversion efficiencies at lower data rates, but the efficiency significantly decreases at high data rates (larger resonance linewidths), making the ring resonator suitable only for low data rate operation. Therefore, our scheme (FPBG)—employing a pump-recycled singly resonant FWM process—is highlighted by its larger signal bandwidth and improved CE. In addition, the CE of the FPBG device can be significantly improved by reducing the waveguide loss. The singly resonant FWM scheme is inherently generic and can be applied across various material platforms, such as Si_3N_4 (see Fig. S4 of the [supplementary material](#)). This versatility highlights its potential to significantly relax both device length and pump power requirements, making it a broadly applicable approach for enhancing FWM performance in diverse photonic systems.

IV. CONCLUSION

In summary, we have successfully demonstrated a singly resonant FWM process utilizing a band-structured FPBG cavity in the AlGaAsOI platform. This approach enables a broadband FWM with high CE, requiring significantly lower absolute pump power and shorter device length compared to conventional single-pass nonlinear waveguides. Moreover, it supports higher data rates than mirroring-resonator-based all-optical wavelength converters. The experimental results show a 16.6 dB enhancement in CE using a 1-mm-long FPBG cavity compared to its waveguide counterpart of the same length. Further reducing propagation loss in the FP cavity

could enhance FWM efficiency even more. Our approach establishes the groundwork for a green and high-speed fully, integrated wavelength converter and facilitates various broadband FWM-enabled nonlinear applications, including quantum optics⁴¹ and Raman spectroscopy.⁴²

SUPPLEMENTARY MATERIAL

See the [supplementary material](#) for calculations on intensity enhancement in cavities, numerical simulations of FWM conversion efficiency, an analysis of DBR's radiation modes, and a numerical investigation of the Si_3N_4 platform.

ACKNOWLEDGMENTS

This work was supported by the European Research Council (Grant No. REFOCUS 853522), the Danish National Research Foundation (SPOC ref. DNRF123), VILLUM FONDEN (Grant No. VIL50469), Innovationsfonden (Grant No. GreenCOM 2079-00040B), the Swedish Research Council (Grant No. VR-2015-00535 to P.A.A.), and the K.A. Wallenberg Foundation (P.A.A.).

AUTHOR DECLARATIONS

Conflict of Interest

The authors have no conflicts to disclose.

Author Contributions

C.Y. and P.Z. contributed equally to this work.

Chaochao Ye: Conceptualization (lead); Data curation (lead); Formal analysis (lead); Investigation (lead); Methodology (lead); Writing – original draft (lead); Writing – review & editing (lead). **Ping Zhao:** Data curation (supporting); Formal analysis (supporting); Investigation (supporting); Resources (equal). **Yang Liu:** Resources (supporting). **Xinda Lu:** Resources (supporting). **Chanju Kim:** Resources (supporting); Writing – review & editing (supporting). **Kresten Yvind:** Formal analysis (supporting); Supervision (supporting); Writing – review & editing (supporting). **Peter A. Andrekson:** Formal analysis (supporting); Funding acquisition (supporting); Supervision (supporting); Writing – review & editing (supporting). **Minhao Pu:** Conceptualization (lead); Formal analysis (lead); Funding acquisition (lead); Project administration (lead); Supervision (lead); Writing – review & editing (lead).

DATA AVAILABILITY

The data that support the findings of this study are available from the corresponding author upon reasonable request.

REFERENCES

- A. E. Willner *et al.*, “All-optical signal processing,” *J. Lightwave Technol.* **32**, 660–680 (2014).
- S. J. B. Yoo, “Wavelength conversion technologies for WDM network applications,” *J. Lightwave Technol.* **14**, 955–966 (1996).
- A. A. I. Ali *et al.*, “First demonstration of optical phase conjugation with real time commercial transceiver,” in *45th European Conference on Optical Communication (ECOC)* (IEEE, 2019).

- ⁴D. Kong *et al.*, “Super-broadband on-chip continuous spectral translation unlocking coherent optical communications beyond conventional telecom bands,” *Nat. Commun.* **13**, 4139 (2022).
- ⁵J. Hansryd *et al.*, “Fiber-based optical parametric amplifiers and their applications,” *IEEE J. Sel. Top. Quantum Electron.* **8**, 506–520 (2002).
- ⁶M. Westlund *et al.*, “Transparent wavelength conversion in fibre with 24 nm pump tuning range,” *Electron. Lett.* **38**, 85–86 (2002).
- ⁷J. Leuthold *et al.*, “Nonlinear silicon photonics,” *Nat. Photonics* **4**, 535–544 (2010).
- ⁸D. Liang and J. E. Bowers, “Recent progress in lasers on silicon,” *Nat. Photonics* **4**, 511–517 (2010).
- ⁹N. Vermeulen *et al.*, “Post-2000 nonlinear optical materials and measurements: Data tables and best practices,” *J. Phys. Photonics* **5**, 035001 (2023).
- ¹⁰P. Zhao *et al.*, “100-Gbps per-channel all-optical wavelength conversion without pre-amplifiers based on an integrated nanophotonic platform,” *Nanophotonics* **12**, 3427–3434 (2023).
- ¹¹J. Riemensberger *et al.*, “A photonic integrated continuous-travelling-wave parametric amplifier,” *Nature* **612**, 56–61 (2022).
- ¹²Z. Ye *et al.*, “Overcoming the quantum limit of optical amplification in monolithic waveguides,” *Sci. Adv.* **7**, eabi8150 (2021).
- ¹³K. Yamada *et al.*, “All-optical efficient wavelength conversion using silicon photonic wire waveguide,” *IEEE Photonics Technol. Lett.* **18**, 1046–1048 (2006).
- ¹⁴L. Ottaviano *et al.*, “Low-loss high-confinement waveguides and microring resonators in AlGaAs-on-insulator,” *Opt. Lett.* **41**, 3996 (2016).
- ¹⁵M. Pu *et al.*, “Efficient frequency comb generation in AlGaAs-on-insulator,” *Optica* **3**, 823–826 (2016).
- ¹⁶M. Pu *et al.*, “Ultra-efficient and broadband nonlinear AlGaAs-on-insulator chip for low-power optical signal processing,” *Laser Photonics Rev.* **12**, 1800111 (2018).
- ¹⁷E. Stassen *et al.*, “Ultra-low power all-optical wavelength conversion of high-speed data signals in high-confinement AlGaAs-on-insulator microresonators,” *APL Photonics* **4**, 100804 (2019).
- ¹⁸F. Morichetti *et al.*, “Travelling-wave resonant four-wave mixing breaks the limits of cavity-enhanced all-optical wavelength conversion,” *Nat. Commun.* **2**, 296 (2011).
- ¹⁹C. Kim *et al.*, “Parity-time symmetry enabled ultra-efficient nonlinear optical signal processing,” *eLight* **4**, 6 (2024).
- ²⁰S. P. Yu *et al.*, “Photonic-crystal-reflector nanoresonators for Kerr-frequency combs,” *ACS Photonics* **6**, 2083–2089 (2019).
- ²¹S. Xie *et al.*, “On-chip Fabry–Perot Bragg grating cavity enhanced four-wave mixing,” *ACS Photonics* **7**, 1009–1015 (2020).
- ²²T. Wildi *et al.*, “Dissipative Kerr solitons in integrated Fabry–Perot microresonators,” *Optica* **10**, 650 (2023).
- ²³C. Kim *et al.*, “Design and fabrication of AlGaAs-on-insulator microring resonators for nonlinear photonics,” *IEEE J. Sel. Top. Quantum Electron.* **29**, 1–13 (2022).
- ²⁴P. Rabiei *et al.*, “Polymer micro-ring filters and modulators,” *J. Lightwave Technol.* **20**, 1968–1975 (2002).
- ²⁵A. N. Kamel *et al.*, “Surface defect effects in AlGaAs-on-insulator photonic waveguides,” *Opt. Express* **31**, 20424–20439 (2023).
- ²⁶S. Grillanda and F. Morichetti, “Light-induced metal-like surface of silicon photonic waveguides,” *Nat. Commun.* **6**, 8182 (2015).
- ²⁷B. Guha *et al.*, “Surface-enhanced gallium arsenide photonic resonator with quality factor of 6×10^6 ,” *Optica* **4**, 218 (2017).
- ²⁸W. Xie *et al.*, “Ultrahigh-Q AlGaAs-on-insulator microresonators for integrated nonlinear photonics,” *Opt. Express* **28**, 32894 (2020).
- ²⁹Y. Long *et al.*, “All-optical wavelength conversion and signal regeneration of PAM-4 signal using a silicon waveguide,” *Opt. Express* **24**, 7158 (2016).
- ³⁰I. Sackey *et al.*, “1024 Tb/s wavelength conversion in a silicon waveguide with reverse-biased p-i-n junction,” *Opt. Express* **25**, 21229 (2017).
- ³¹C. Lacava *et al.*, “Ultra-low-power silicon photonics wavelength converter for phase-encoded telecommunication signals,” *SPIE Proc.* **9752**, 975211 (2016).
- ³²F. Luan *et al.*, “Dispersion engineered As₂S₃ planar waveguides for broadband four-wave mixing based wavelength conversion of 40 Gb/s signals,” *Opt. Express* **17**, 3514 (2009).
- ³³F. Da Ros *et al.*, “Low-penalty up to 16-QAM wavelength conversion in a low loss CMOS compatible spiral waveguide,” in *Optical Fiber Communications Conference and Exhibition (OFC)* (IEEE, 2016), p. Tu2K.5.
- ³⁴C. Koos *et al.*, “All-optical high-speed signal processing with silicon–organic hybrid slot waveguides,” *Nat. Photonics* **3**, 216–219 (2009).
- ³⁵M. P. Nielsen *et al.*, “Giant nonlinear response at a plasmonic nanofocus drives efficient four-wave mixing,” *Science* **358**, 1179–1181 (2017).
- ³⁶B. Corcoran *et al.*, “Ultracompact 160 Gbaud all-optical demultiplexing exploiting slow light in an engineered silicon photonic crystal waveguide,” *Opt. Lett.* **36**, 1728 (2011).
- ³⁷F. Li *et al.*, “All-optical wavelength conversion for 10 Gb/s DPSK signals in a silicon ring resonator,” *Opt. Express* **19**, 22410 (2011).
- ³⁸Z. Yan *et al.*, “Broadband continuous-wave mid-infrared wavelength conversion in high-Q silicon microring resonators,” *Photonics Res.* **12**, 2257–2264 (2024).
- ³⁹X. Hu *et al.*, “Graphene-silicon microring resonator enhanced all-optical up and down wavelength conversion of QPSK signal,” *Opt. Express* **24**, 7168 (2016).
- ⁴⁰A. Pasquazi *et al.*, “All-optical wavelength conversion in an integrated ring resonator,” *Opt. Express* **18**, 3858 (2010).
- ⁴¹L. Duan *et al.*, “Visible-telecom entangled-photon pair generation with integrated photonics: Guidelines and a materials comparison,” *ACS Photonics* **12**, 118–127 (2025).
- ⁴²N. M. Lüpken *et al.*, “Spontaneous four-wave mixing in silicon nitride waveguides for broadband coherent anti-Stokes Raman scattering spectroscopy,” *Opt. Lett.* **45**, 3873 (2020).